JOURNAL OF SPACECRAFT AND ROCKETS
Vol. 46, No. 6, November–December 2009

Star-Body Waveriders with Multiple Design Mach Numbers

Stephen Corda*
University of Tennessee Space Institute, Tullahoma, Tennessee 37388

DOI: 10.2514/1.43933

A new type of star-body waverider is presented that has multiple design Mach numbers. A limitation of typical waverider configurations is that they have a single design Mach number, where the shock wave is attached to all of its leading edges. At this design Mach number, there is no flow spillage and the static pressure on the compression surfaces is maximized. The center wedge sections of the new star bodies have different flow deflection angles corresponding to different design Mach numbers, thereby generating lift and side force that can be used for increased range and maneuver capability. A baseline Mach 6, conventional star body, an equivalent volume cone, and three multiple-design-Mach-number star bodies are analyzed using three-dimensional, full Navier–Stokes computational fluid dynamics for Mach numbers of 4, 5, 6, 7, and 8 and an altitude of 100,000 ft. As expected, the conventional, single-design-Mach-number star body has higher skin-friction drag, lower wave drag, and lower total drag than the equivalent volume cone. Because the volumes of the multiple-design-Mach-number star bodies are greater than that of the cone, they have higher total drag than the cone, but the wave drag and drag coefficient are lower than the equivalent cone for some of the new configurations at higher Mach numbers. Before performing the analysis, it was assumed that the star body sectors at an on-design flow condition would have the greatest pressure levels. However, the computational fluid dynamics analysis showed that the star-body sectors with the maximum flow deflection (center wedge) angle produced the highest pressures, even at offdesign flow conditions, where three-dimensional effects and pressure loss due to detached shocks and flow spillage are present. The asymmetric, two-, and triple-design-Mach-number star bodies produced lift that can be used for downrange and cross-range capability.

Nomenclature

C_D	=	drag coefficient
C_L	=	lift coefficient
C_p	=	pressure coefficient
D	=	drag, lb_f
L	=	lift, lb_f
L/D	=	lift-to-drag ratio
l	=	configuration length, ft
M_D	=	design Mach number
Re_l	=	Reynolds number based on configuration length
S_{base}	=	configuration base area, ft^2
S_{wet}	=	configuration wetted surface area not including base area, ft^2
V	=	configuration volume, ft^3
$V^{2/3}/S_{\text{wet}}$	=	volumetric efficiency
β	=	shock wave angle, deg
γ	=	ratio of specific heats for air
θ	=	flow deflection (wedge) angle, deg

I. Introduction

WAVERIDER configurations are typically designed for optimum performance at a single, freestream Mach number [1]. At this design Mach number, the waverider "rides" atop its shock wave, the flow between the shock wave and the waverider lower surface is fully contained, and there is no flow spillage around the vehicle leading edges. This high-pressure, fully contained flow on the waverider lower surface results in superior aerodynamic performance, such as higher lift-to-drag ratio L/D over conventional, nonwaverider hypersonic configurations. At offdesign Mach numbers, the shock wave is detached from the waverider leading edges and there is flow spillage, resulting in lower aerodynamic performance. Waverider designs have been pursued for their high hypersonic L/D advantage, although disadvantages, such as low volumetric efficiency and the requirement for aerodynamically sharp leading edges, are pragmatic design considerations.

The caret wing, conceived by Nonweiler [2], is perhaps the simplest waverider shape and is derived from two-dimensional, supersonic, and hypersonic wedge flow. The caret wing waverider rides atop the planar shock wave generated by the configuration's centerline, two-dimensional wedge (Fig. 1). As shown in Fig. 1, the caret wing waverider is constructed by forming a center wedge with an angle equal to the two-dimensional wedge angle θ and "drawing" straight leading edges that ride on top of the planar shock wave. At the on-design Mach number, the shock wave is fully attached to the caret wing leading edges, there is no flow spillage, and the flow beneath the caret wing is two-dimensional and thus easily analyzable with simple techniques, such as Newtonian impact theory. At offdesign Mach number conditions, the shock wave is no longer attached to the caret wing leading edges, the flow is three-dimensional, and these simpler analysis techniques are not accurate.

By joining several caret wing shapes together, a class of waveriders known as wedge-derived star bodies can be created. These star-body waveriders have a star-shaped cross section with any number of star points or leading-edge fins. Previous researchers [3–5] have shown that, at on-design conditions, these star-body shapes have lower wave drag than right circular cones with equivalent length and volume. Although the present research focuses on wedge-derived star-body shapes, it is applicable to star bodies with any other longitudinal flow turning shape, such as conical or power-law body derived star bodies [6]. With their lower wave drag in comparison to simple cones, these star-body configurations have been investigated for use as supersonic and hypersonic missile, projectile, and forebody shapes. Gonor et al. [7] investigated the use of star-body configurations as the forebody/inlet of a scramjet propulsion system.

Previously designed star body shapes have a single design Mach number; that is, all of the star-body centerline wedge sections have the same wedge deflection angle, producing a shock-on-fin leading-edge condition at only one Mach number. At any Mach number other than the design Mach number, the shock wave is no longer attached to the fin leading edges, there is flow spillage, and a subsequent decrease in aerodynamic efficiency. Also, because all of the star-body wedge sections have the same flow deflection angle, these

Received 19 February 2009; revision received 16 August 2009; accepted for publication 19 August 2009.

*Chairman and Associate Professor, Aviation Systems Program, 411 B.H. Goethert Parkway, Mail Stop 20; scorda@utsi.edu. Senior Member AIAA.

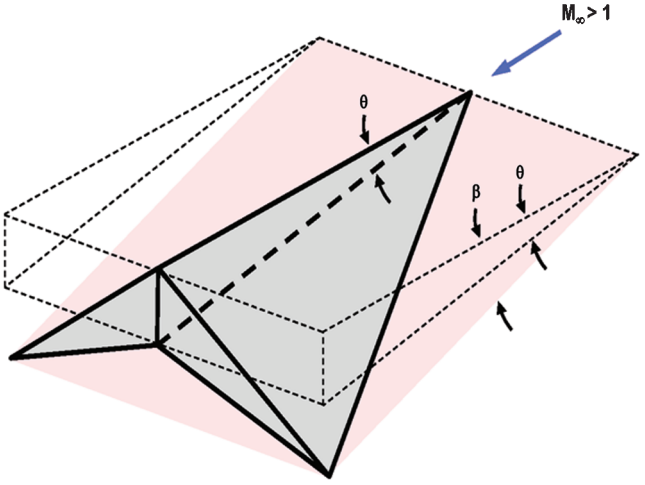

Fig. 1 Waverider concept for a simple caret wing (θ = flow deflection or wedge angle, β = shock wave angle).

axially symmetric configurations produce a finite aerodynamic drag, but do not produce any lift or side force, at zero angle of attack.

The present research represents the first attempt to create star-body waveriders with multiple design Mach numbers. Star-body waveriders are particularly suitable because the multiple caret wing segments may be individually tailored for a different design Mach number. By choosing a different design Mach number for each center wedge section, the star body can produce lift and side force and may result in a more optimum aerodynamic configuration "tailoring" over a Mach number range. These multiple-design-Mach-number star-body configurations would still be suitable for low-wave-drag missiles, projectiles, and forebodies/inlets, with the added capability of producing lift and side force as desired. The multiple-design-Mach-number star-body concept is depicted in Fig. 2, where the bottom and side sectors are assumed to have different design Mach numbers. (Note that Fig. 2 is a depiction to enhance this discussion and does not represent analysis results. The shock waves for only two sectors of the star body are depicted for clarity.) If the star body is flying at a freestream Mach number equal to the design Mach number of the bottom sector, the shock wave is attached to all of the bottom sector's leading edges (shown in red) while the shock wave is detached (shown in yellow) on the side sector, because it is at an offdesign condition.

Initially, it was assumed that it might be aerodynamically advantageous to rotate the star body such that it is riding atop the wedge section with a design Mach number that is equal to or closest to the freestream Mach number. It was thought that the on-design Mach number sector would provide the highest static pressure because the shock wave is fully attached and there is no flow spillage. As will be seen, the computational results do not support this assumption. Several exemplary star-body waveriders with multiple-design Mach numbers are presented and analyzed using three-dimensional, full Navier–Stokes (FNS) computational fluid dynamics with no assumptions of configuration axisymmetry. The aerodynamics of the multiple-design-Mach-number star bodies are compared with those of conventional star bodies with a single design Mach number and an equivalent volume cone.

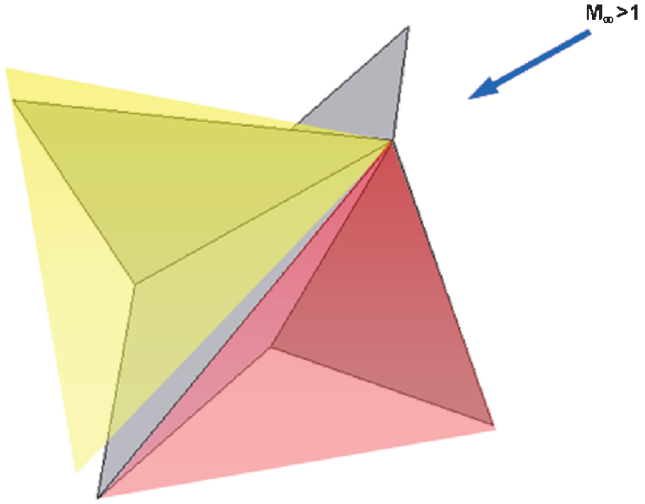

Fig. 2 Star-body waverider depicting on-design and offdesign shock conditions for the bottom (red) and the side (yellow) sectors, respectively.

II. Configuration Descriptions and Design Methodology

The configurations designed and analyzed in the present study are described next. The design methodologies used in creating the single- and multiple-design-Mach-number star bodies are detailed. The configurations considered include a Mach 6, conventional star body with a single design Mach number, an equivalent volume cone, and three different multiple-design-Mach-number star bodies. The choice of Mach 6 as the design point allowed the variation of lower and higher Mach numbers in the design study without consideration of high-temperature effects. The conventional, single-design-Mach-number star body was considered the baseline configuration for the present study to evaluate the relative merits and/or deficiencies of the other configurations.

All of the configurations were assumed to be forebody shapes, that is, it was assumed that an afterbody or nozzle would be attached to the star-body base to provide a complete vehicle configuration. Therefore, the effect of the base area was neglected in the following analyses so that the aerodynamics of the forebodies alone could be compared. The length of every configuration was assumed to be 6 ft, loosely based on a reasonable dimension that might be considered for a missile type forebody.

A. Sharp Leading-Edge Assumption

Similar to previous analytical and experimental investigations of star-body and other waverider shapes [1–7], the present analysis assumes that the star-body waveriders have aerodynamically sharp leading edges. Although this assumption is advantageous from an aerodynamic performance perspective, it is not realistic in terms of practical heat transfer considerations. All of the waverider shapes will require some amount of leading-edge bluntness to mitigate hypersonic stagnation line heating and withstand mechanical loads.

Although a detailed design and analysis of waverider blunt leading edges is beyond the scope of the present study, previous investigators have focused on this specific detailed design issue [8–11]. Vanmol and Anderson [8] performed a detailed study of waverider heat transfer, including the effects of leading-edge bluntness. Flight conditions of Mach 5, 10, 15, and 20, at low and high dynamic pressures of 423.2 lb_f/ft^2 and 2116 lb_f/ft^2, respectively, were analyzed. The waverider leading edge was assumed to be made of carbon–carbon with a refractory metal, heat pipe active cooling system. The maximum wall temperature and heat transfer for this leading–edge concept was 1900 K and 10.3 MW/m^2, respectively.

At Mach 5 and the maximum wall temperature of 1900 K, the leading-edge radius could be as small as 1 mm without the need for active cooling. At Mach 10 and the maximum wall temperature of 1900 K, a leading-edge radius of 10 mm required the use of the active cooling system. At Mach 20, the maximum heat transfer at the waverider leading edge and the nose tip were estimated to be 2.0 MW/m^2 and 9.5 MW/m^2, respectively. Both heating conditions were predicted to be within the capabilities of the active cooling capabilities.

In considering the effects of the leading-edge bluntness on the waverider aerodynamics, the inviscid leading-edge drag was found to be approximately 4–8% of the total inviscid drag. Vanmol and Anderson [8] concluded that the waverider concept, in terms of increased aerodynamic performance over conventional, non-waverider configurations, is still viable when the leading-edge heat

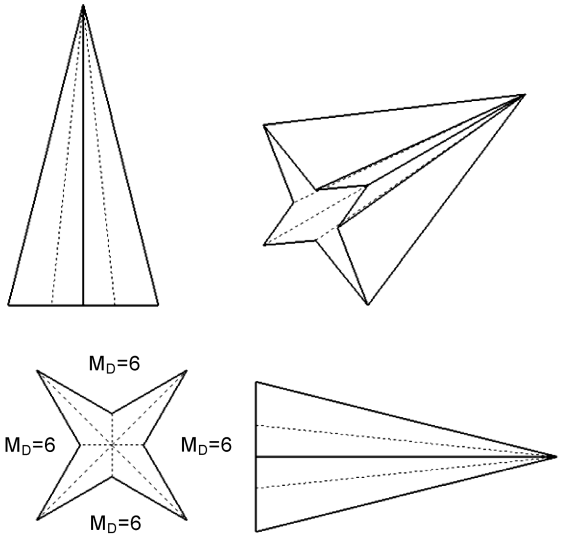

Fig. 3 Star-body with one design Mach number, $M_D = 6$.

transfer effects are taken into consideration. It is expected that the sharp leading-edge assumption will lead to slightly optimistic aerodynamic performance of all configurations, but the results of the comparative analysis of the different star-body configurations should still be valid.

B. Conventional Star Body with a Single Design Mach Number

In general, a star-body geometry can be uniquely defined by specifying the number of caret wing sectors or fins, the configuration length l, the center wedge angle θ, and the desired design Mach number M_D. At the design Mach number, the planar shock wave produced by the center wedge is fully attached to the fin leading edges. Assuming the weak solution, the shock wave angle β, corresponding to the design Mach number and the center wedge angle, is uniquely defined through the θ-β-M relation [12] [Eq. (1)]:

$$\tan\theta = 2\cot\beta\left[\frac{M_D^2\sin^2\beta - 1}{M_D^2(\gamma + \cos 2\beta) + 2}\right] \tag{1}$$

Figure 3 shows a four-fin, star-body configuration with a single design Mach number of 6, designated as the baseline Mach 6 star body. The choice of four caret wing sectors or fins is arbitrary and star bodies with any number of fins could be constructed using the present methodology. The star-body geometry is constructed by merging four caret wings with each caret wing cross section occupying a 90 deg sector. Every center wedge angle is the same and the configuration is symmetric such that the opposite fins are perfectly aligned with each other. The design Mach number, the center wedge angle, and the length were specified as Mach 6, 6 deg, and 6 ft, respectively. The design shock wave angle of 13.982 deg and the specified configuration length of 6 ft result in a star-body fin height of 1.494 ft.

Other details of the Mach 6 star-body geometry are given in Table 1, including the volume V, wetted surface area S_{wet}, base area S_{base}, planform area, and volumetric efficiency. The wetted surface area in Table 1 is the configuration total wetted surface area not including the base area. The volumetric efficiency is defined as the volume to the two-thirds power, divided by the wetted surface area as defined earlier, $V^{2/3}/S_{\text{wet}}$.

C. Equivalent Volume Cone

For comparison purposes, an equivalent volume cone configuration was defined. The cone has the same length and volume as the baseline Mach 6 star body. The equivalent volume assumption produced a cone with a 10.345 deg semi-apex angle. Table 1 provides details of the equivalent cone geometry. Note that the baseline, Mach 6 star body has approximately twice the surface area of the equivalent volume cone. This results in the star body having a volumetric efficiency that is approximately half of the equivalent volume cone. Initially it was thought that a cone with an equivalent volumetric efficiency might provide a better comparison, but this results in an impractical, needlelike cone with a semi-apex angle of only 1.323 deg, surface area of 2.613 ft^2, and volume of 0.1206 ft^3.

D. Multiple-Design-Mach-Number Star Bodies

In general, the center wedge angle of each caret wing sector of the star body can be set to a different value corresponding to a different design Mach number. Based on the present selection of a four-sector star shape, up to four different design Mach numbers could be used to define the four center wedge angles. Three different multiple-design-Mach-number star-body shapes were analyzed in the present study, two different types of two-design-Mach-number star bodies and a triple-design-Mach-number star body. A four-design-Mach-number star body was also designed, but not analyzed, because the extreme asymmetry of this configuration was not considered practical.

The three multiple-design-Mach-number star-body configurations are shown in Figs. 4–6. All of these configurations have four caret wing sectors and four leading-edge fins, similar to the baseline Mach 6 star body. The specification of the design Mach number for each sector is somewhat arbitrary in the present study, as other combinations could be created. The present configuration selections attempts to provide a range of different types of multiple-design-Mach-number star bodies to analyze and compare.

By changing the design Mach number of one of the four wedge sections of the baseline, single-design-Mach-number star body, the asymmetric, two-design-Mach-number star body shown in Fig. 4 was created. Here, the top wedge section has a design Mach number of 8 while the remaining three sectors have design Mach numbers of 6. The symmetric, two-design-Mach-number star body is shown in Fig. 5, with opposite sectors having the same design Mach numbers of 6 and 8. This symmetric configuration will result in a finite drag, but zero lift and side force, at zero angle of attack. Figure 6 shows the star body with three design Mach numbers of 6, 7, and 8. Two opposite sectors have the same design Mach number of 7 while the other two opposite sectors have design Mach numbers of 6 and 8. Again, many variations of multiple-design-Mach-number star bodies can be created by varying the number of wedge sections or fins and the design Mach number assigned to each wedge.

The multiple-design-Mach-number star bodies were constrained to have the same length and shock wave angles as the baseline, single-design-Mach-number star body. With these geometric constraints, the center wedge angles can be calculated using Eq. (1), assuming the fixed shock wave angle of 13.982 deg and the selected design Mach number. Table 2 shows the calculated center

Table 1 Configuration data[a]

Configuration[a]	Volume, ft^3	Surface area[b], ft^2	Base area, ft^2	Planform area, ft^2	Volumetric efficiency
Mach 6, one M_D star body	7.537	41.58	3.769	1.450	0.09244
Equivalent volume cone	7.537	20.99	3.769	1.450	0.1832
Asymmetric, two M_D star body	8.313	40.95	4.157	1.450	0.1002
Symmetric, two M_D star body	9.089	40.31	4.545	1.450	0.1080
Three M_D star body	9.250	40.13	4.625	1.450	0.1098

[a]All configurations have a length of 6 ft.
[b]Forebody surface area only, excludes surface area of base.

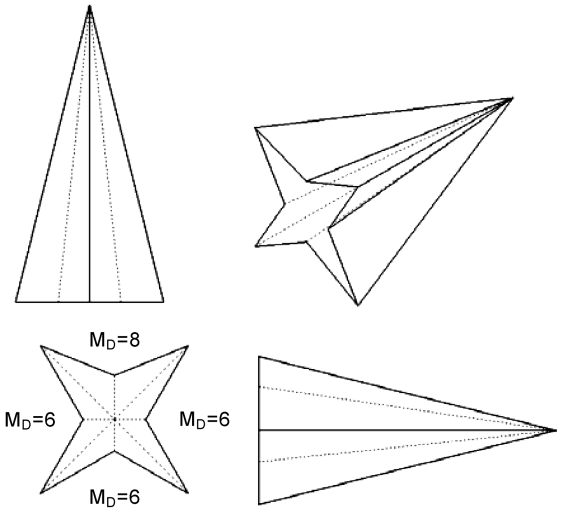

Fig. 4 Asymmetric star body with two design Mach numbers, $M_D = 6$ and 8.

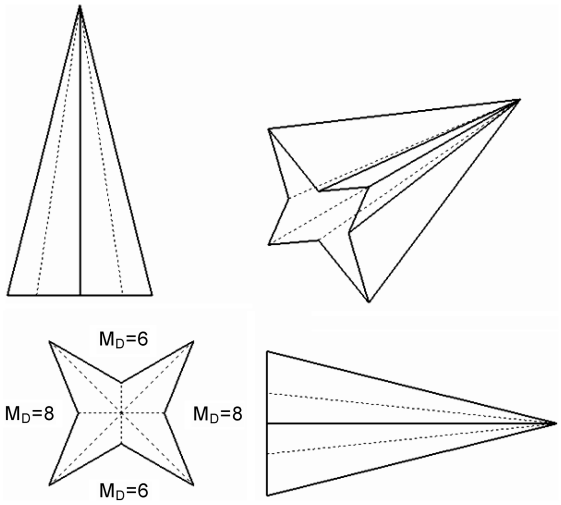

Fig. 5 Symmetric star body with two design Mach numbers, $M_D = 6$ and 8.

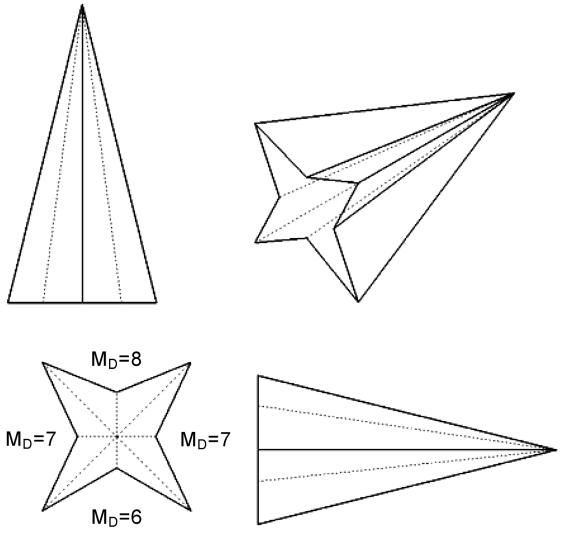

Fig. 6 Star-body with three design Mach numbers, $M_D = 6$, 7, and 8.

Table 2 Wedge angles producing 13.982 deg shock wave angle

Mach no.	Wedge angle, deg
5	3.575
6	6.000
7	7.477
8	8.440

wedge angles corresponding to the 13.982 deg shock wave angle and design Mach numbers of 5, 6, 7, and 8. It should be emphasized that, because the shock wave angle is fixed for any design Mach number, the leading edges of adjacent sectors with different design Mach numbers are forced to be identical. There is no mismatch in the leading-edge line between sectors with different design Mach numbers.

Because, for a fixed shock wave angle, the wedge angle increases with increasing Mach number, the higher design Mach number specification leads to caret wing segments with higher volume. The star-body wetted surface areas are approximately twice that of the equivalent volume cone and their volumetric efficiencies are approximately half that of the cone (Table 1). It may have been possible to match the star-body volumes by varying the configuration length, but it was desired to maintain a constant Reynolds number, based on the length, at each Mach number. Note that, although the volumes and base areas of the star bodies differ, their surface areas differ by a maximum of about 3%. As shown in Table 1, all of the star bodies with multiple design Mach numbers have significantly greater volumes and base areas than the baseline star body. The volume and base area of the triple-design-Mach-number star body are both 22.7% greater than the baseline star body. Note that, although the multiple-design-Mach-number star bodies have larger volumes, their forebody, wetted surface areas are comparable. Note also that the multiple-design-Mach-number star bodies have increased volumetric efficiency over the baseline star body. For example, the triple-design-Mach-number star body has an 18.8% greater volumetric efficiency than the baseline star body.

III. Computational Fluid Dynamic Analysis Method

The configurations were analyzed by solving the three-dimensional, FNS equations using computational fluid dynamics. The computational fluid dynamic (CFD) calculations were performed using the SolidWorks® Flow Simulation [13] software package. The time-dependent, three-dimensional, full Navier–Stokes equations are solved using a finite volume method where the governing equations are discretized in a conservative form. The code uses a spatially rectangular, solution adaptive meshing that increases the mesh density in the high gradient flow regions as the solution develops. The solution mesh was refined periodically, after the number of iterations required for a fluid particle to travel from the entrance to the exit of the computational domain. Converged solutions were typically reached after approximately 3000–4000 iterations.

Three-dimensional calculations were performed on the complete configurations, with no symmetry boundary conditions assumed, even for the equivalent volume, simple cone, and geometrically symmetric star bodies. A typical three-dimensional computational mesh is shown in Fig. 7 for the baseline star body at a freestream Mach number of 6. Only half the mesh is depicted in Fig. 7 for clarity. Again, note that the complete three-dimensional configuration was meshed and computed, even though the star body has geometric planes of symmetry. The mesh around the body is a Cartesian cube with the inflow and exit planes located at the nose and base of the star body, respectively. Preliminary computations were performed with the inflow plane upstream of the star body nose to confirm that the nose shock waves were fully attached. Also, the lateral boundaries were located far enough from the body such that the shock waves exited the downstream boundary only. Typical mesh densities were

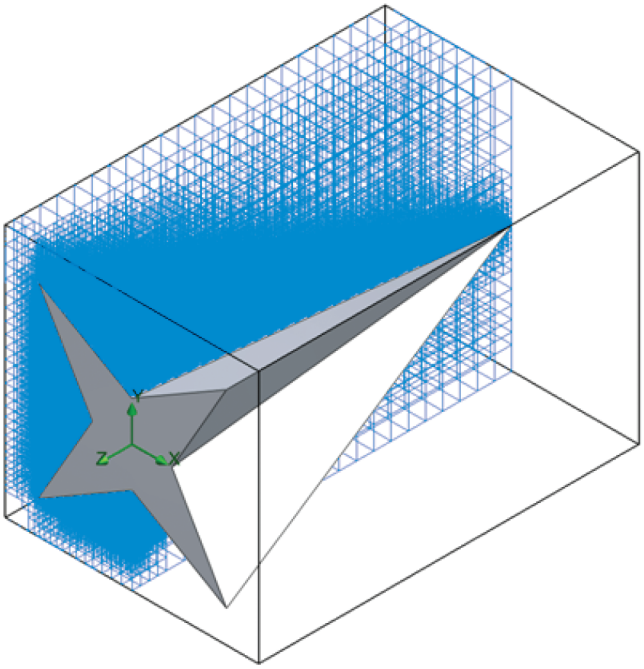

Fig. 7 Three-dimensional mesh for star body with one design Mach number, $M_D = 6$ (mesh shown for half of body for clarity).

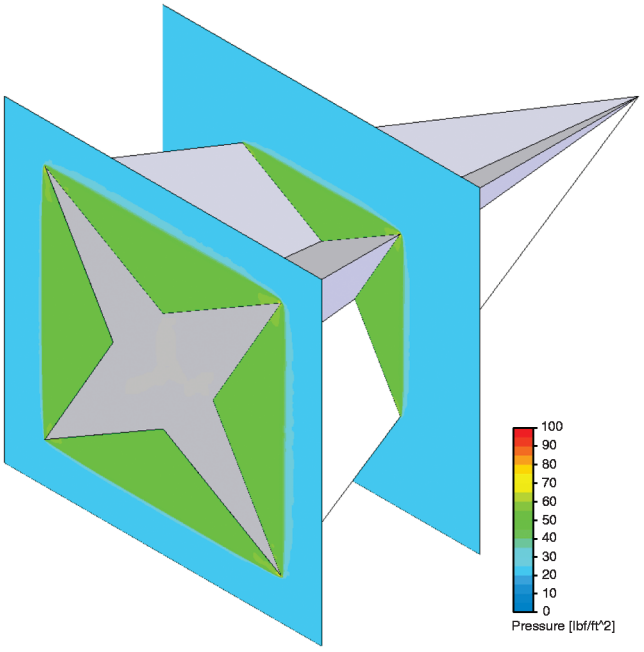

Fig. 8 Pressure contours from 3-D FNS CFD for a single-design-Mach-number star body at Mach 6.

over one million mesh cells for each solution. Because the mesh is rectangular everywhere in the computational domain, there are partial cells located at the solid/fluid boundaries that are refined as required to resolve the wall boundary geometry.

For the computations, the entire flow was assumed to be fully turbulent. A two-equation k-ε turbulence model is used in the code. No slip, adiabatic wall boundary conditions were applied at the configuration solid surfaces.

The inflow boundary was assumed to be a uniform freestream flow at the specified Mach number and altitude. Because each configuration was considered a forebody shape, the outflow boundary of the computational domain was at the base of the body. This assumption eliminated the need to obtain the unsteady, separated base flow solution and greatly reduced the computational time required for convergence. The flow at the outflow boundary was always supersonic and not separated, so there was no loss in fidelity in using this boundary condition. Also, the omission of the base region is not considered to reduce the applicability of the present analysis, because the forebody assumption is probably a more realistic geometric configuration.

IV. Results and Discussion

Analyses were performed on five different configurations, the baseline Mach 6, single-design-Mach-number star body, an equivalent volume right circular cone, and three multiple-design-Mach-number star bodies. The configurations were analyzed at freestream Mach numbers of 4, 5, 6, 7, and 8, all at an altitude of 100,000 ft. The angle of attack and angle of sideslip were assumed to be zero. The freestream flight conditions used in the analyses are given in Table 3.

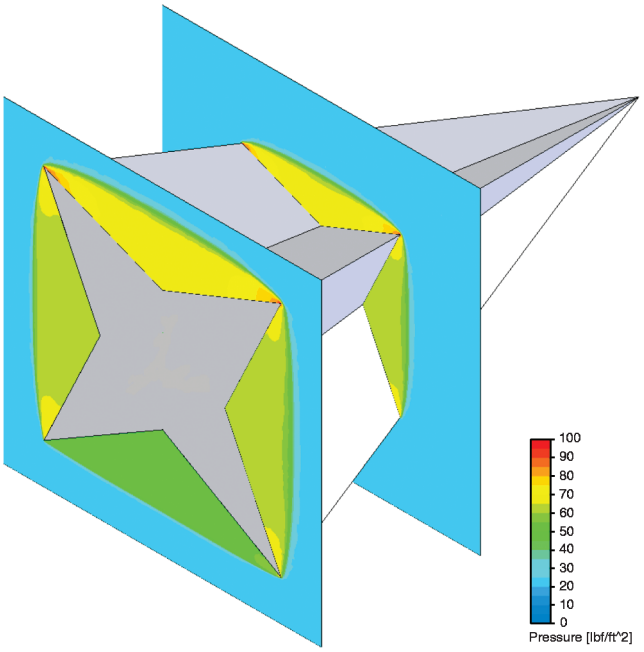

Fig. 9 Pressure contours from 3-D FNS CFD for three-design-Mach-number star body at Mach 6.

Characteristic physical features of the three-dimensional, viscous computational fluid dynamic solutions are shown by the pressure contour, cross section plots in Figs. 8 and 9 for the single- and triple-design-Mach-number star bodies, respectively. The pressure

Table 3 Freestream flow conditions analyzed

Mach no.	Altitude, ft	Pressure, lbs/ft^2	Temperature, °R	Dynamic pressure, lbs/ft^2	Reynolds no., Re_l based on length
4	100,000	23.085	418.79	258.6	2.455×10^6
5	100,000	23.085	418.79	404.0	3.069×10^6
6	100,000	23.085	418.79	581.7	3.682×10^6
7	100,000	23.085	418.79	791.8	4.296×10^6
8	100,000	23.085	418.79	1034.2	4.910×10^6

contours are shown at two cross section locations, at the body base location, and 2 ft upstream of the base. The CFD results in Figs. 8 and 9 are both at a freestream Mach number of 6. The triple-design-Mach-number star body is oriented as shown in Fig. 6, with the Mach 6 wedge on the bottom, the two Mach 7 wedges on the left and right sides, and the Mach 8 wedge on the top.

For the single-design-Mach-number star body, the computation correctly predicts that the shock wave is fully attached to each fin and the high-pressure flow behind the planar shock waves is fully contained between each set of fins. The pressure between each pair of fins is seen to be equal and constant.

As seen in Fig. 9 for the triple-design-Mach-number star body, the planar shock wave is attached to the bottom fins where the design Mach number is 6. The flow is fully contained and there is no flow spillage around the two bottom fins. Because the freestream Mach number of 6 is below the design Mach numbers of 7 and 8 for the sides and top of this configuration, respectively, the shock waves are detached and there is flow spillage between the fin segments. Despite this shock detachment, the flow spillage is localized near the fin leading edges and the high, constant static pressure is still fairly well preserved throughout the sector. These fundamental flow characteristics were evident in all of the computational solutions for the various star-body configurations. The three-dimensional effects produced by the offdesign Mach number conditions were localized to the fin leading edges and the highest static pressure levels were obtained in the sectors with the largest center wedge angles, even at offdesign Mach numbers. Therefore, there would be no need to rotate the star-body configurations, as originally assumed, to orient the body so that the on-design Mach number sector matched the freestream Mach number. In general, the multiple-design-Mach-number star bodies produce lift when the sector with the highest design Mach number (largest center wedge angle) is on the bottom, regardless of the freestream Mach number.

A. Comparison of Predicted Drag

The total drag for each configuration versus Mach number is shown in Fig. 10. Total drag increases with increasing Mach number for all of the bodies. As expected, the star body with a single design Mach number has a lower total drag than the equivalent volume cone over the Mach number range, ranging from 2.4% less total drag than the cone at Mach 4 and increasing to 20.9% less at Mach 8.

Although the drag comparison between the single-design-Mach-number star body and the cone is based on equivalent volume, the same cannot be said when compared with the other star bodies. As shown in Table 1, the volumes and base areas are significantly different for the various star bodies, with the single-design-Mach-number star body having the smallest volume. Because the total drag scales directly with the configuration volume, the single-design-Mach-number star body has the lowest total drag. The triple-design-Mach-number star body has the largest volume and the highest total drag. The symmetric, two-design-Mach-number star body, with a slightly lower volume, has a slightly lower drag than the triple-design-Mach-number star body. The asymmetric, two-design-Mach-number star body has a volume approximately midway between the volumes of the single- and triple-design-Mach-number star bodies, respectively, and therefore a total drag approximately equidistant between the lowest and highest star body total drags.

In general, a star body will have a higher skin-friction drag than an equivalent volume cone, due to the greater wetted surface area. Note that all of the star bodies in the present analysis have approximately twice the wetted surface area of the cone. Despite this higher skin-friction drag, the wave drag of the star body can be significantly lower than a cone, resulting in lower total drag. For example, at Mach 6, the single-design-Mach-number star body has a skin-friction drag component that is 132% greater than the equivalent volume cone, whereas its wave drag component is 17.0% lower. The lower wave drag results in the single-design-Mach-number star body having a total drag that is 10.7% lower than that of the cone. The calculated wave drag and skin-friction drag components are shown for each configuration in Figs. 11 and 12, respectively. The drag calculations from the Taylor-Maccoll cone flow solution [14] are shown in Fig. 11 for the equivalent volume cone. Note that the total drag is dominated by the wave drag. The skin-friction drag is an order of magnitude lower than the wave drag. The relative wave drag comparisons in Fig. 11 are similar to those for the total drag in Fig. 10. The CFD cone flow solutions for wave drag are nearly identical to the Taylor-Maccoll solution, ranging from 1.22% less than the Taylor-Maccoll solution at Mach 4 to 0.91% less at Mach 8.

The trends are quite different for the skin-friction drag shown in Fig. 12. The cone has the lowest skin-friction drag, roughly half that of all the star bodies. Three of the star bodies have similar magnitudes of the skin-friction drag. The skin-friction drag of the asymmetric, two-design-Mach-number star body lies approximately midway between the values for the cone and the other star bodies.

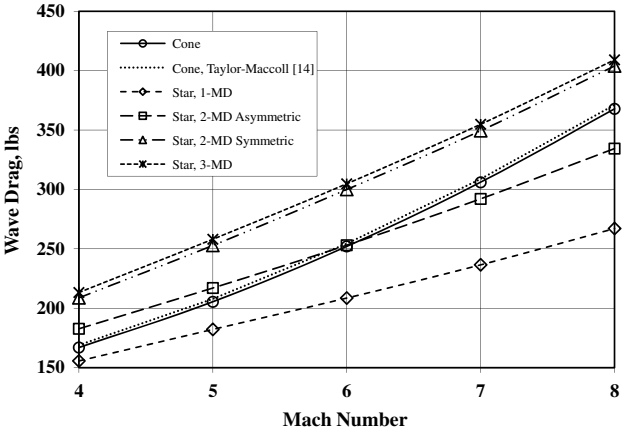

Fig. 11 Comparison of wave drag.

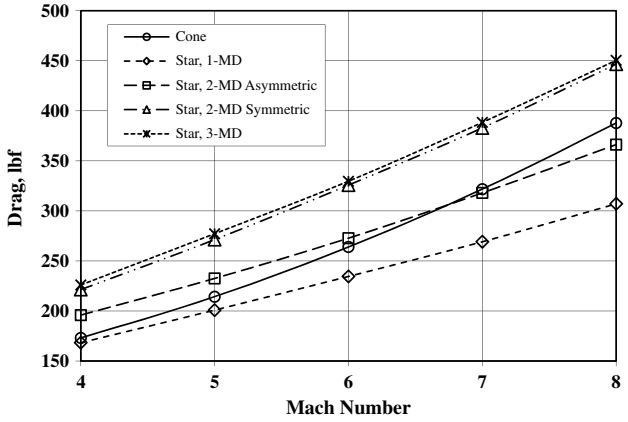

Fig. 10 Comparison of total drag.

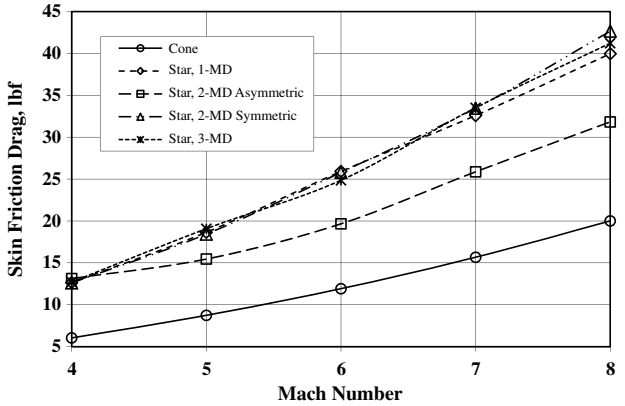

Fig. 12 Comparison of skin-friction drag.

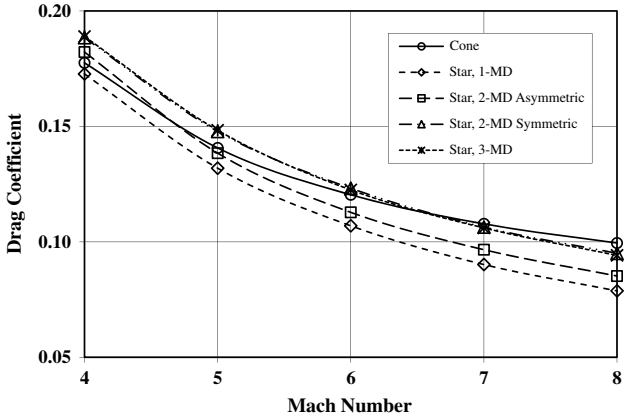

Fig. 13 Comparison of drag coefficient.

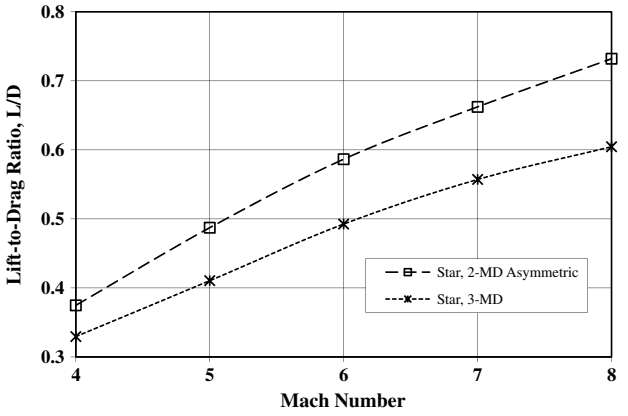

Fig. 15 Lift-to-drag ratio of lift-producing star bodies.

The drag coefficients for each configuration versus Mach number are shown in Fig. 13. The reference area used to calculate the drag coefficient is the configuration base area. In comparing the different configurations, the trends in the drag coefficient follow the trends for the total drag. The single-design-Mach-number star body has the lowest drag coefficient over the Mach number range. The three-design-Mach-number star body has the highest drag coefficient from Mach 4 to about 5.6, with the cone having the largest drag coefficient between Mach 5.6 and 8.

B. Comparison of Predicted Lift

The total lift generated by the different configurations is shown in Fig. 14. The cone and symmetric star bodies do not produce any lift force because the freestream flow is at zero angle of attack. The asymmetric, two-design-Mach-number star body and the triple-design-Mach-number star body are predicted to produce approximately the same amount of lift versus Mach number. By comparing Figs. 4 and 6, this might be expected because both configurations have a Mach 6 wedge and a Mach 8 wedge on opposite sides. The two configurations have different design Mach number wedges on the left and right quadrants, the two-design-Mach-number star body having Mach 6 wedges and the three-design-Mach-number star body having Mach 7 wedges. Note that, although Figs. 4 and 6 show the Mach 8 and Mach 6 sectors on the top and bottom, respectively, the higher static pressure is obtained on the Mach 8 sector throughout the Mach number range, therefore the lift force vector would be directed downward in these figures. Because the computations were performed at zero angle of attack and because there were no precomputation assumptions as to the resultant force vectors, the orientation of the sectors for the computations was not important. The lift data in Fig. 14 assume that the Mach 8 sector is on the bottom for the asymmetric, two-design-Mach-number star body (Fig. 4) and the triple-design-Mach-number star body (Fig. 6). The lift for these star bodies increases with increasing Mach number, from about 70 lb_f at Mach 4 to about 20 lb_f at Mach 8.

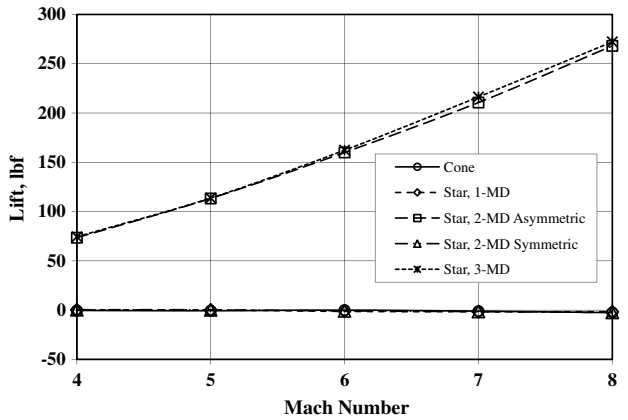

Fig. 14 Comparison of total lift.

The lift-to-drag ratio L/D for the two lift-producing star-body configurations versus Mach number is shown in Fig. 15. The L/D of the asymmetric, two-design-Mach-number star body is greater than that for the three-design-Mach-number star body due to its lower total drag versus Mach number. The L/D increases with increasing Mach number for both configurations. The magnitudes of the lift-to-drag ratio are relatively low, below an L/D of one, but these positive L/D values do provide downrange and cross-range capability, whereas the symmetric star bodies cannot.

V. Conclusions

New types of star-body waveriders with multiple design Mach numbers were designed and analyzed using three-dimensional, full Navier–Stokes computational fluid dynamics. Five star-body configurations were analyzed, all with four fins: a star body with a single design Mach number of 6, a laterally symmetric star body with two-design Mach numbers of 6 and 8, an asymmetric star body with two-design Mach numbers of 6 and 8, a star body with three design Mach numbers of 6, 7, and 8, and a right circular cone with a volume equivalent to the single-design-Mach-number star body. All configurations were analyzed for flight at 100,000 ft and Mach numbers of 4, 5, 6, 7, and 8.

As has been demonstrated by previous investigators, the conventional, single-design-Mach-number star body has higher skin-friction drag, lower wave drag, and lower total drag than the equivalent volume cone. Because of their significantly greater volumes and wetted surface areas, the multiple-design-Mach-number star bodies had higher total drag than the equivalent cone, but the wave drag and drag coefficient is lower than the equivalent cone for some of these new configurations at higher Mach numbers.

The asymmetric, two-design, and triple-design-Mach-number star-body configurations produced lift that can be used for downrange and cross-range capability. Before conducting the present computational analysis, it was assumed that the star body sectors at an on-design flow condition would have the greatest static pressure levels to contribute to this lift. The CFD analysis did not support this assumption, rather it showed that the star body sectors with the maximum flow deflection (center wedge) angle produced the highest static pressures, even at offdesign flow conditions. The CFD results showed that the pressure losses due to offdesign Mach number conditions were localized to regions along the star body leading edges where the shock wave was detached and there was flow spillage. Despite this, the static pressure between the body and the planar shock wave was preserved at a near constant and high level. Therefore, to produce lift or side force, the asymmetric, multiple-design-Mach-number star body must be oriented such that the sector with the higher design Mach number (larger center wedge angle) is opposite the desired direction of force, that is, if lift is desired, the larger center wedge angle must be on the bottom of the configuration.

References

[1] Corda, S., and Anderson, J. D., Jr., "Viscous Optimized Hypersonic Waveriders Designed from Axisymmetric Flow Fields," *AIAA 26th Aerospace Sciences Meeting*, Reno, Nevada, AIAA Paper 88-0369, Jan. 1988.

[2] Nonweiler, G. T., "Aerodynamic Problems of Manned Space Vehicles," *Journal of the Royal Aeronautical Society*, Vol. 63, 1959, pp. 521–528.

[3] Chernyi, G. G., and Gonor, A. L., "Transverse Contour of Minimum Pressure Drag," *Theory of Optimum Aerodynamic Shapes*, edited by A. Miele, Academic, New York, 1965, Chap. 19, pp. 283–295.

[4] Gonor, A. L., Kazakov, M. N., and Shvets, A. I., "Drag Measurements on Star-Shaped Body at $M = 6$ and 8," *Fluid Dynamics*, Vol. 3, No. 1, 1968, pp. 64–66.
doi:10.1007/BF01016240

[5] Gonor, A. L., Kazakov, M. N., Shvets, A. I., and Shein, V. I., "Aerodynamic Characteristics of Star-Shaped Bodies at Supersonic Velocities," *Fluid Dynamics*, Vol. 6, No. 1, 1971, pp. 86–89.
doi:10.1007/BF01045911

[6] Sabean, J. W., Lewis, M. J., Mee, D., and Paull, A., "Performance Study of a Power Law Starbody," *Journal of Spacecraft and Rockets*, Vol. 36, No. 5, Sept.–Oct. 1999, pp. 646–652.
doi:10.2514/2.3496

[7] Gonor, A. L., Khakine, V. A., Blankson, I. M., Goldfeld, M. A., and Starov, A. V., "Numerical and Experimental Studies of the Supersonic Star-Shaped Inlet with Fuel Injection," *46th AIAA Aerospace Sciences Meeting*, AIAA Paper 2008-95, Jan. 2008.

[8] Vanmol, D. O., and Anderson, J. D., Jr., "Heat Transfer Characteristics of Hypersonic Waveriders with an Emphasis on the Leading Edge Effects," NASA CR 189586, March 1992.

[9] Blosser, M. L., Blankson, I. M., Schoerke, S., Brunson, D., and Hagseth, P., "Wing Leading Edge Design Concepts for Air-Breathing Hypersonic Waveriders," *32nd AIAA Aerospace Sciences Meeting & Exhibit*, AIAA Paper 94-0379, Jan. 1994.

[10] Blosser, M. L., Blankson, I. M., Schoerke, S., Brunson, D., and Hagseth, P., "Wing Leading Edge Design Concepts for Air-Breathing Hypersonic Waveriders," *Journal of Aircraft*, Vol. 32, No. 2, March–April 1995, pp. 307–312.
doi:10.2514/3.46717

[11] Pan, J., Yan, C., Geng, Y., and Wu, J., "Aerothermodynamics of the Waverider Applying Artificially Blunted Leading Edge Concept," *47th AIAA Aerospace Sciences Meeting*, AIAA Paper 2009-748, Jan. 2009.

[12] Anderson, J. D., Jr., *Modern Compressible Flow*, 3rd ed., McGraw–Hill, New York, 2003, Chap. 4.

[13] SolidWorks® Flow Simulation 2009, Dassault Systemes SolidWorks Corp., Veilzy, France, 2009.

[14] Anderson, J. D., Jr., *Modern Compressible Flow*, 3rd ed., McGraw–Hill, New York, 2003, Chap. 10.

M. Miller
Associate Editor